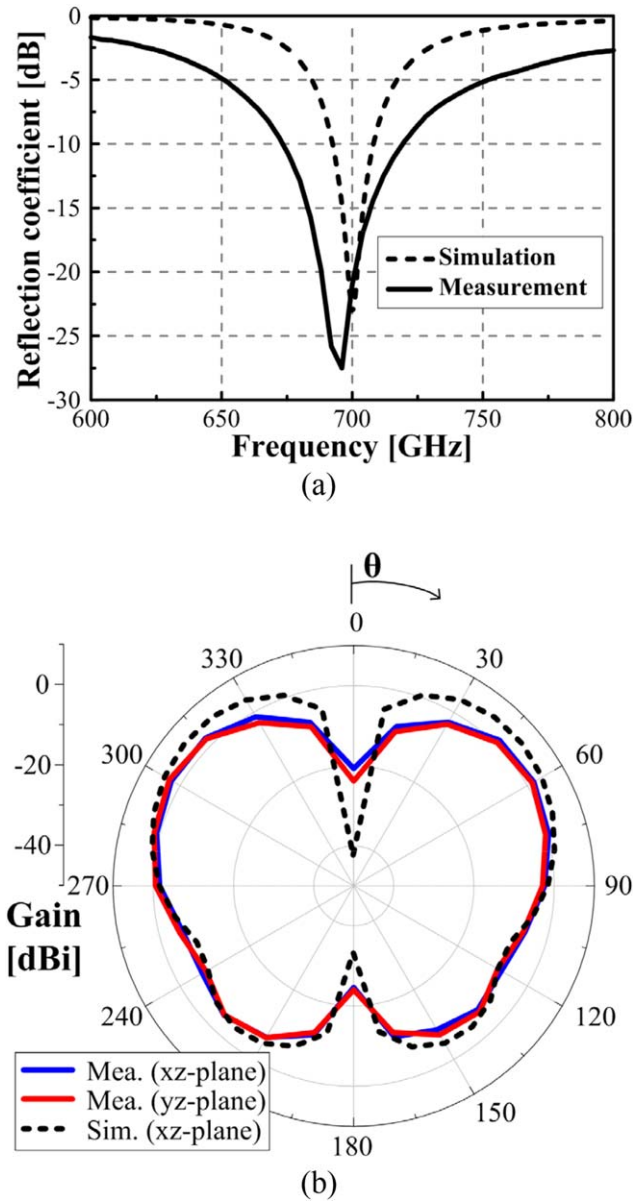

Figure 7 Simulated and measured reflection coefficients and radiation pattern results: (a) reflection coefficients and (b) far-field radiation patterns. [Color figure can be viewed at wileyonlinelibrary.com]

printing and was fastened at the ground with PC nuts and bolts. Simulated and measured results of the flush-mounted HMCPA exhibited monopole-like radiation characteristics. Therefore, the proposed flush-mounted monopolar patch antenna is a good candidate for UAV, aircraft, and automotive applications.

ACKNOWLEDGMENTS

This work was supported by the research fund of Signal Intelligence Research Center supervised by Defense Acquisition Program Administration and Agency for Defense Development of Korea.

REFERENCES

1. S.D. Keller, W.O. Coburn, and S.J. Weiss, Efficient electromagnetic modeling of bent monopole antenna on aircraft wing using FEKO, *Proc 2009 the Third European Conf. Antennas Propag. (EuCAP)*, Berlin, March 2009, pp. 2226–2228.
2. B.T. Strojny and R.G. Rojas, Integration of conformal GPS and VHF/UHF communication antennas for small UAV applications, *Proc 2009 the Third European Conf. Antennas Propag. (EuCAP)*, Berlin, March 2009, pp. 2488–2492.
3. S.D. Keller, Wire-Frame monocone antenna for direction-finding applications on unmanned aerial vehicle platform, IEEE Antennas Propag Mag 53 (2011), 56–65.
4. R.W.S. Harrison and M. Jessup, A novel log periodic implementation of a 700 MHz – 6 GHz slant polarised fixed-beam antenna array for direction finding applications, *Proc 2012 the 42rd European Microw Conf (EuMC)*, Amsterdam, Oct. 2012, pp. 727–730.
5. F. Sultan, H. Ali, M.S. Sharawi, and D.N. Aloi, A printed V-shaped circular antenna array for direction finding applications, *Proc. 2012 the 6th European Conf. Antennas Propag. (EuCAP)*, Prague, March 2012, pp. 3115–3118.
6. J. Tak, and J. Choi, A low-profile dipole array antenna with monopole-like radiation for on-body communications, KIEES J Electromagn Eng Sci 15 (2015), 245–249.
7. L. Scorrano, A. Manna, and F. Trotta, A novel dual-polarized broadband UHF blade antenna for avionic applications, *Proc. 2015 IEEE-APS Topical Conf. Antennas Propag. Wireless Commun. (APWC)*, Turin, Sept. 2015, pp. 1179–1180.
8. A. Patrovsky and R. Sekora, Structural integration of a thin conformal annular slot antenna for UAV applications, *Proc. 2010 Loughborough Antennas Propag. Conf. (LAPC)*, Loughborough, Nov. 2010, pp. 229–232.
9. S. Kang, K. Jang, J. Jeon, I. Yang, K. Kahng, S. Mok, and J. Anguera, Wideband and low-profile metamaterial antennas for aircrafts and automobiles, *Proc. 2014 the 8th European Conf. Antennas Propag. (EuCAP)*, The Hague, Apr. 2014, pp. 976–977.
10. L. Economou, and R.J. Langley, Patch antenna equivalent to simple monopole, IET Electron Lett 33 (1997), 727–729.
11. J. Liu, Q. Xue, H. Wong, H.W. Lai, and Y. Long, Design and analysis of a low-profile and broadband microstrip monopolar patch antenna, IEEE Trans Antennas Propag 61 (2013), 11–18.
12. J. Tak, D. Kang, and J. Choi, A tapered double cross patch antenna for dual-band monopole-like radiation, Microwave Opt Technol Lett 56 (2014), 2929–2933.
13. J. Tak, and J. Choi, Circular-ring patch antenna with higher order mode for on-body communications, Microwave Opt Technol Lett 56 (2014), 1543–1547.
14. J. Tak, S. Lee, and J. Choi, All-textile higher order mode circular patch antenna for on-body to on-body communications, IET Microwave Antennas Propag 9 (2015), 576–584.

PARAMETRIC MACROMODELING OF INTEGRATED INDUCTORS FOR RF CIRCUIT DESIGN

F. Passos,[1] Y. Ye,[2] D. Spina,[2] E. Roca,[1] R. Castro-López,[1] T. Dhaene,[2] and F.V. Fernández[1]

[1] Universidad de Sevilla, Instituto de Microelectrónica de Sevilla, CNM-CSIC, Seville, Spain; Corresponding author: moreira@imse-cnm.csic.es

[2] Department of Information Technology, IDLab, Ghent University - imec, Gent, Belgium

Received 24 October 2016

ABSTRACT: *Nowadays, parametric macromodeling techniques are widely used to describe electromagnetic structures. In this contribution, the application of such parametric macromodeling techniques to the design of integrated inductors and radio-frequency circuit design is investigated. In order to allow such different operations, a new modeling methodology is proposed, which improves the modeling accuracy when compared to former techniques. The new methodology is tailored to the unique characteristics of the devices under study. The obtained*

parametric macromodel is then used in a synthesis methodology and in the design of a voltage controlled oscillator in a 0.35-μm CMOS technology. © 2017 Wiley Periodicals, Inc. Microwave Opt Technol Lett 59:1207–1212, 2017; View this article online at wileyonlinelibrary.com. DOI 10.1002/mop.30498

Key words: *integrated inductor; parametric macromodeling; RF design; single-objective optimization; VCO*

1. INTRODUCTION

In recent years many models have been developed for integrated inductors because of their important role in radio frequency integrated circuits (RF ICs). Most of these models are based on lumped-element circuits, like the π-model [1], the double π-model [2], and the T-model [3]. However, these models present accuracy issues, with modeling errors that may exceed 10% [1,2] or rely on complex extraction techniques from fabricated samples [3].

Nowadays, black-box approaches based on parametric macromodeling techniques establish a reliable solution for studying generic linear and passive electromagnetic (EM) structures [4–6]. Parametric macromodeling techniques model the transfer function of such EM structures, which can be expressed in different forms (e.g., admittance, impedance, or scattering parameters), preserving at the same time fundamental physical properties, such as causality, stability, and passivity, so that a complete characterization both in the frequency and time domains is obtained [5,6].

The focus of this letter is the modeling of integrated inductors over a large design space, developing a model suitable for different tasks (e.g., inductor synthesis, design space exploration, circuit design, etc.). In this scenario, not only an accurate estimation of the inductors' transfer function is needed (which can later be used to derive the inductor *S*-parameters and used for circuit design), but also the main inductor performances used in inductor synthesis (inductance L and quality factor Q) have to be accurately modeled, since these are the performances used by designers to set optimization objectives and constraints.

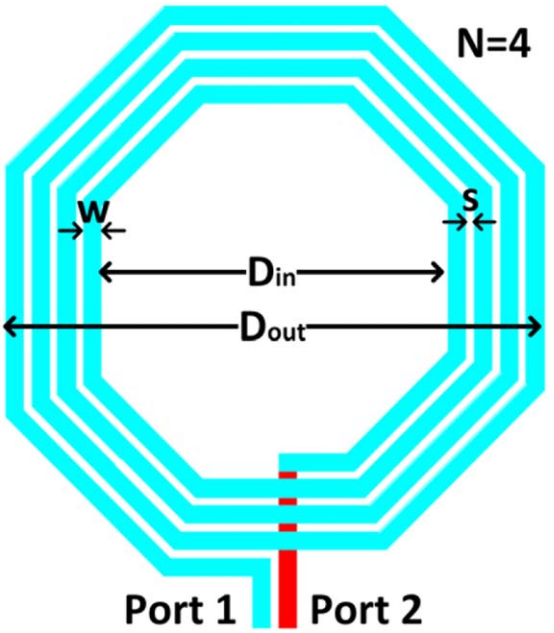

Figure 1 Layout of an octagonal five turns spiral inductor. [Color figure can be viewed at wileyonlinelibrary.com]

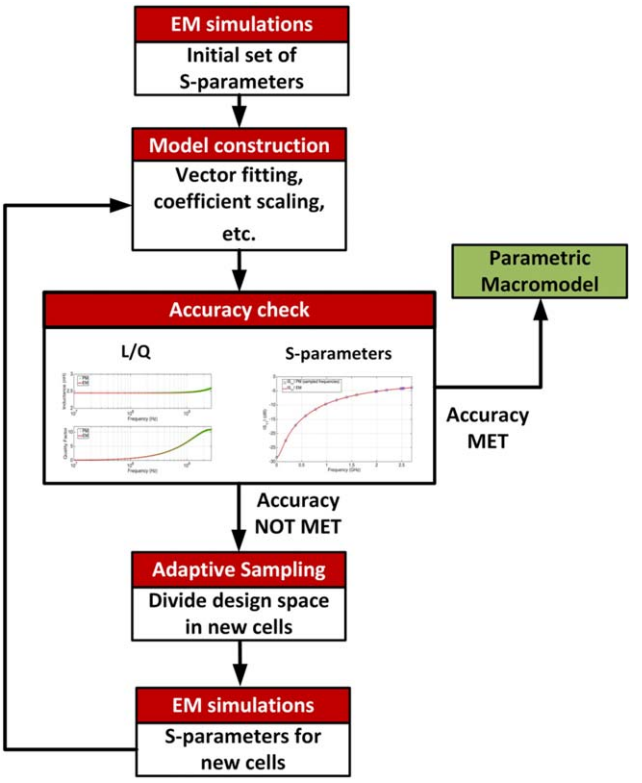

Figure 2 Flowchart for the creation of the proposed parameterized macromodel, with the accuracy check on different parameters. [Color figure can be viewed at wileyonlinelibrary.com]

In this work the parametric macromodeling technique presented in Ref. [5] and the sequential sampling strategy described in Ref. [6], which are able to build a stable and passive macromodel over the entire design space, have been combined and modified in order to allow one to use different levels of accuracy over the design space, in order to alleviate the computational cost of building the model in areas where inductors are less suitable for circuit design. Second, the new modeling technique presents an accurate estimation of not only *S*-parameters but also L and Q. The accuracy improvement of all performances is obtained by applying a new error measurement strategy during the sequential sampling technique. This strategy is tailored to the unique characteristics of integrated inductors.

The new modeling methodology, which is described in Section 2, is then used in Section 3 to synthetize the inductor required for the design of a voltage controlled oscillator (VCO). To the best of the authors' knowledge, this is the first time a parametric macromodeling technique for integrated inductors is used in circuit design. Finally, conclusions are drawn in Section 4.

2. PARAMETRIC MACROMODELING OF INTEGRATED INDUCTORS

The integrated spiral inductor topology modeled in this work is shown in Figure 1. The technology selected was a 0.35-μm CMOS technology, for which the process information required for EM simulation was available. The methodology presented in this work is completely independent of the inductor topology and technology, being therefore very flexible.

Separate models are built for inductors with different number of turns N. In each case, the design space for model building is defined by the inner diameter D_{in} and turn width w, which vary in the following ranges: $D_{in} \in [10, 300]$ μm and $w \in [5, 25]$

TABLE 1 Maximum Relative Error in the Estimation of *L* and *Q* at 2.5 GHz for 4936 Test Inductors

N	*Mabs* (dB)	Model S		Model SLQ	
		MRL(%)	*MRQ*(%)	*MRL*(%)	*MRQ*(%)
1	−60	2.26	9.06	1.58	3.51
2	−60	2.03	5.10	2.03	5.10
3	−50	1.45	6.31	1.45	2.85
4	−50	2.09	5.18	1.28	2.36
5	−50	1.14	2.04	1.14	2.04

μm. The maximum area of the inductors is limited by a reasonably large outer diameter D_{out} of 400 μm, whereas the spacing between inductor turns s is maintained fixed at the minimum allowed by the technology, 2.5 μm, since no performance improvement is achieved by increasing this value [7]. In order to build the models, the S-parameters of the selected samples are evaluated over 17 frequency samples in the range [0.0001, 2.7] GHz. The number of frequency samples used has a direct impact on the accuracy/efficiency trade-off of the modeling process: using more frequency points provides more information about the behavior of the integrated inductor, but it will lead to an increase on computational time, since EM simulations must be performed for each frequency sample.

The performance parameters L and Q can be directly computed from the inductor S-parameters as

$$Z_{\text{eq}}=50\frac{(1+S_{11})(1+S_{22})-S_{12}S_{21}}{(1+S_{11})(1+S_{22})+S_{12}S_{21}}$$
$$L=\frac{\text{Im}\,(Z_{\text{eq}})}{2\pi f} \quad Q=\frac{\text{Im}\,(Z_{\text{eq}})}{\text{Re}\,(Z_{\text{eq}})} \tag{1}$$

Samples for model construction are evaluated with the EM simulator Keysight ADS Momentum [8]. Inductances below 50 pH are not considered, since such components are not used in RF design.

The entire modeling technique can be seen in the flowchart presented in Figure 2. The first step to compute the parametric macromodel is to electromagnetically simulate the samples corresponding to the corners of the design space and a model is built using these samples. Starting from these initial data samples, a corresponding set of frequency-dependent rational models is built by means of the vector fitting (VF) technique [9]. After this initial phase, a set of stable and passive frequency-dependent rational models, called root macromodels, is computed. Each of these root macromodels models a single section (cell) of the design space defined by its corners. Afterwards, amplitude and frequency scaling system coefficients are computed for the root macromodels of each cell by means of an optimization procedure and then properly parameterized by positive interpolation operators [5].

Afterwards, the model accuracy of each cell is checked. If the model error is below a defined error threshold for a given cell, the model is marked as accurate enough. If the error is above the selected threshold in a given cell, this cell is divided into subcells by means of an adaptive sampling technique. The whole training-validation process is automatically and recursively applied in each subcell until we have a set of accurate local models that ensure the desired error threshold in every cell of the design space. All the generated local models form the complete parametric macromodel for the entire design space.

It becomes clear that one of the key steps in the modeling process is which error measure to use and its threshold value. In this work, two error measurement techniques will be compared in order to demonstrate the validity of the improved accuracy check proposed in this work. In previous reported models [5], only the error in estimating the transfer function of the device under study was considered. A possible choice is using the maximum absolute error between the S-parameter obtained via EM simulations and the macromodel in the entire frequency range (*Mabs*), which was adopted in Ref. [5] for the entire design space. However, the accuracy of L and/or Q can be very sensitive to errors in the estimation of the S-parameters. Table 1 shows the maximum relative error of L (*MRL*) and Q (*MRQ*) at 2.5 GHz calculated over a set of 4936 test inductors (different from the inductors used for model training) when the model is built using only the *Mabs* error measure of the S-parameters (which we will denote as model S). It should be mentioned that inductors with different number of turns can be modeled with different *Mabs* thresholds in order to achieve superior accuracy. Note that for inductors up to four turns the *MRQ* is always higher than 5%. This result confirms that a small error in the estimation of the S-parameters can correspond to a high relative error in e.g., estimating Q.

It is therefore clear that a new strategy must be adopted in order to obtain accurate modeling results for L and Q. With previous techniques, such as model S, it is impossible to apply different error measurements to different areas of the design space.

Thus, the only solution to increase the accuracy of the model is to reduce the error threshold for the *Mabs*, e.g., from −50 to −70 dB. However, this will lead to over-sampling the entire (w, D_{in}) design space, which is not a practical solution.

Therefore, the new methodology proposed in this letter consists in adopting an error measure based on S-parameters as well as L and Q and also allow the designer to set different error measures for different areas of the design space. With the proposed approach, we guarantee an accurate estimation not only

TABLE 2 Number of Samples Used to Build the SLQ Model

N	Number of (W, D_{in}) samples used for model training and verification			Extensive validation (Offline validation)			
				100 kHz		2.5 GHz	
	Training	Online validation	CPU Time	$\bar{\varepsilon}_L$ (%)	$\bar{\varepsilon}_Q$ (%)	$\bar{\varepsilon}_L$ (%)	$\bar{\varepsilon}_Q$ (%)
1	123	88	0.94h	0.27	1.25	0.28	0.91
2	253	177	10.03h	0.20	0.74	0.21	0.66
3	207	150	11.30h	0.22	1.01	0.22	0.69
4	197	145	18.81h	0.22	0.99	0.21	0.55
5	140	102	20.23h	0.22	0.88	0.19	0.46

L and Q mean relative errors for model SLQ (extensive verification).

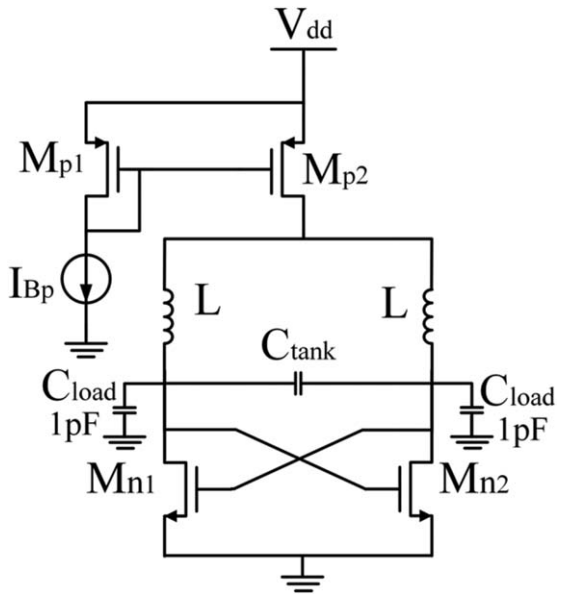

Figure 3 VCO single-differential topology

of the *S*-parameters, but also of *L* and *Q* with the desired accuracy in the entire design space. In this work, the selected relative error threshold values in the estimation of *L* and *Q* are

- ε_L, ε_Q <6% for $L \in$[0.05, 0.5] nH;
- ε_L, ε_Q <3% for $L >$0.5nH.

where ε_L and ε_Q are the relative error values of *L* and *Q*, respectively. The threshold value selected (3%) results in a good trade-off between accuracy and computational time (EM simulation of new samples) for the final models. For values of $L < 0.5$ nH, a higher threshold value is considered to reduce the number of EM simulations needed for the model construction, since these inductors are rarely used in circuit design. The parametric macromodels computed by means of the proposed error measure (model SLQ) are capable of modeling the performances of integrated inductors more accurately, therefore helping to improve the design of RF circuits, as will be shown in next section.

The results presented in Table 1 show a significant improvement with respect to the corresponding model S computed with the same *Mabs* error threshold for the *S*-parameters. Furthermore, Table 2 shows the mean relative error of *L* and *Q* ($\bar{\varepsilon_L}$ and $\bar{\varepsilon_Q}$) for an extensive validation study using the 4936 test inductors. The total number of (w, D_{in}) samples used to compute the parametric macromodels, including the samples used to verify the model accuracy during the automatic model building stage, are also included in Table 2, as well as the CPU time needed to simulate the inductors used for training and validation.

3. INDUCTOR SYNTHESIS AND VCO DESIGN

In this Section a single-differential VCO (illustrated in Figure 3) is designed to demonstrate the advantages of the proposed modeling strategy (model SLQ) when compared to the former technique (model S) and other methods used by RF designers (e.g., EM simulations).

When designing circuits where inductors are needed (e.g., VCOs), designers usually look for inductors with a given inductance and high quality factors (e.g., by increasing the quality factor of the inductor, the VCO phase noise is decreased). In order to obtain optimal inductors, an optimization process will be performed using three different performance evaluators: the EM simulator ADS Momentum, the S and the SLQ models. The optimization results and efficiency will then be compared. The optimization algorithm used was PSO [10] (with 40 individuals and 200 generations) and the objective was to achieve an inductor with $L = 2 \pm 0.05$ nH while maximizing the quality factor, within a maximum area of 165 μm^2.

However, in order to properly design inductors for RF circuits, a highly complex set of constraints must be applied.

TABLE 3 Results for Inductor Synthesis Using Three Different Performance Evaluators

	N	Din (μm)	*w* (μm)	*L*@2.5 GHz	ΔL (%)	*Q*@2.5 GHz	ΔQ (%)	CPU time
EM	3	111	7.25	1.99	–	10.32	–	192.2h
SLQ	3	111	7.4	1.99	**0.04**	10.34	**0.34**	4 min
S	3	110	7.6	1.98	**0.71**	9.75	**6.21**	4 min

TABLE 4 Values of the Components Used in VCO Simulation

	$W_{n1,2}$ (μm)	$l_{n1,2}$ (μm)	W_{p1} (μm)	W_{p2} (μm)	$l_{p1,2}$ (μm)	I_{BP} (mA)	C_{tank} (fF)
EM	75	0.35	50	150	3	1	397
SLQ	75	0.35	50	150	3	1	395
S	75	0.35	50	150	3	1	403

TABLE 5 VCO Performances Using the Previously Synthetized Inductors

	Phase Noise (dBc/Hz)	Δ (%)	f_{osc} (GHz)	Δ (%)	V_{out} (V)	Δ (%)
EM	−124.11	–	2.50	–	1.01	–
SLQ	−124.12	0.01	2.50	0.02	1.01	0.27
S	−123.68	0.37	2.50	0.36	0.97	4.40

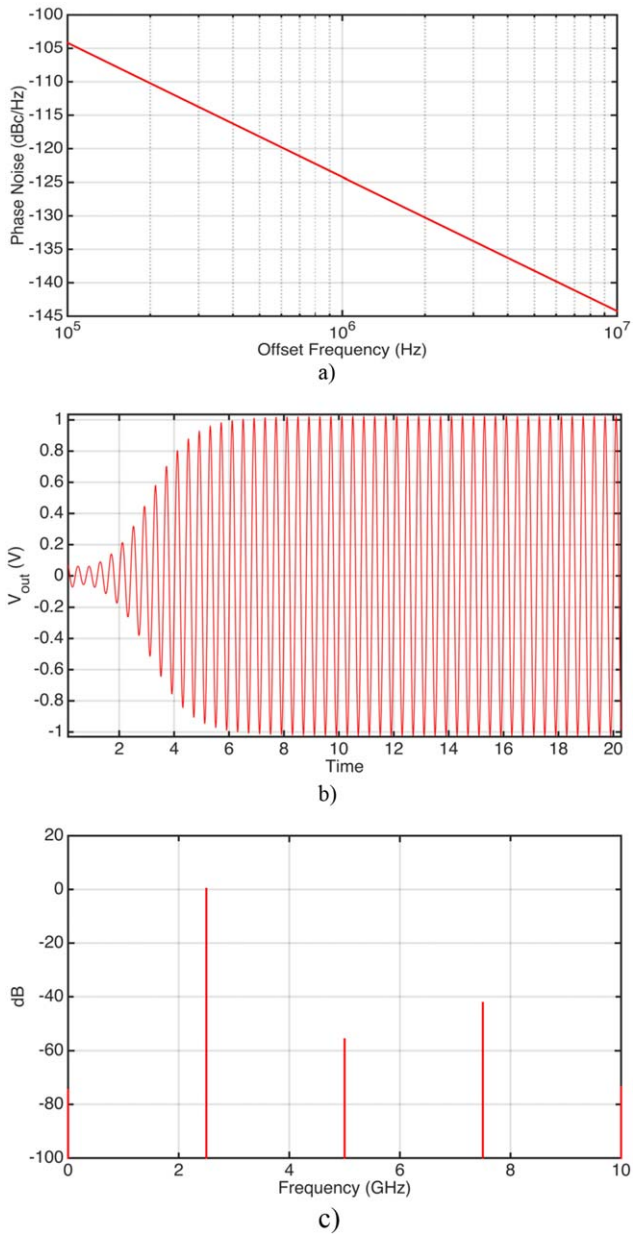

Figure 4 Performances of the VCO designed using the SLQ model. (a) VCO phase noise, (b) VCO transient simulation, and (c) VCO output voltage spectrum. [Color figure can be viewed at wileyonlinelibrary.com]

These constraints are specified in the following set of equations [7]:

$$\begin{cases} area < 400\mu\text{m}\times 400\mu\text{m} \\ \left|\frac{L_{@WF}-L_{@WF+0.05\text{GHz}}}{L_{@WF}}\right| < 0.01 \\ \left|\frac{L_{@WF}-L_{@WF-0.05\text{GHz}}}{L_{@WF}}\right| < 0.01 \\ \left|\frac{L_{@WF}-L_{\text{at }0.1\text{GHz}}}{L_{@WF}}\right| < 0.05 \\ Q_{@WF+0.05GHz}-Q_{@WF} > 0 \end{cases} \quad (2)$$

where $L_{@WF}$ and $Q_{@WF}$ are the inductance and quality factor at the working frequency (WF) and $L_{@WF\pm0.05GHz}$ and $Q_{@WF\pm0.05GHz}$ are the inductance and quality factor at the $WF\pm0.05$GHz.

These constraints are used in order to ensure that the inductance is sufficiently flat from around DC to slightly above the working frequency, that the self-resonance frequency of the inductor is sufficiently above the working frequency and finally, that the deviations in L and Q because of process variations are minimized [7]. These constraints are another reason why such accurate L and Q estimations are needed: with errors of e.g., 6% (as obtained with the model S), these constraints may be wrongly calculated and optimization may lead to areas where constraints are not actually met.

Table 3 presents the results of the three optimizations using the different performance evaluators. The CPU time needed for each process is also given in Table 3. Notice that the model generation also requires the CPU times shown in Table 2 but that is just a one-time investment and the resulting models can be used as many times as necessary, therefore the time used to build the model should not be accounted for in this optimization.

All techniques achieve similar inductors, however, models S and SLQ are much more efficient than the optimization using EM simulations. The quality factor of the inductor obtained with model S is lower than the other methods and the inductance obtained with the model SLQ and the EM simulations is closer to the desired value (2 nH).

Afterwards, the inductors obtained with the models were simulated electromagnetically in order to inspect the model errors (see columns ΔL and ΔQ in Table 3). It can be concluded that the optimization using model S did not converge to the same inductor as model SLQ because of its higher error prediction (around 6% in Q). Therefore, using the model S can lead the RF designer into selecting suboptimal inductors for a given application.

Each of the inductors obtained in the synthesis processes were then used in order to design different VCOs in a 0.35-μm CMOS technology with an oscillation frequency ($f$osc) of 2.5 GHz and a supply voltage $V_{\text{dd}} = 1.5$ V.

The design variables of each designed VCOs can be observed in Table 4, where, $W_{n1,2}$ are the transistor gate widths of the differential pair, $l_{n1,2}$ are the channel lengths of these transistors, W_{p1}, W_{p2} are the gate widths of the current mirror used to polarize the circuit and l_{p1}, l_{p2} are their channel lengths. Finally, C_1 is the capacitor used in the VCO tank. The inductors used in each method are the ones obtained in the synthesis (see Table 3).

Although, the C_{tank} value had to be changed among the different VCOs (in order to obtain the desired f_{osc}), all the other components were fixed at the same value in order to inspect the influence of the different obtained inductors in the performances of the VCO.

All circuit simulations have been carried out with Cadence *SpectreRF* circuit simulator [11]. The results are shown in Table 5. It can be observed that the VCO performances are superior (lower phase noise and higher output voltage) when the inductor obtained with the model SLQ is used, which is because of the higher quality factor inductor obtained by model SLQ during the optimization stage, which proves that the new modeling strategy brings advantages during circuit design.

The inductors obtained by the models have a certain error, as shown in Table 3. Therefore, the inductors were simulated electromagnetically and also used in circuit simulation in order to compare the VCO performance deviations by using the models. The deviations are shown in Table 5 and denoted by Δ. It can be observed that the model SLQ provides an outstanding accuracy (better than the model S) for all VCO performances, as negligible shifts with respect to the corresponding VCO performances obtained with a EM-simulated inductor. On the other

hand, the VCO performances obtained with the inductor synthesized with model S show almost 5% error for the output voltage (V_{out}), which is a key performance (the output voltage of the VCO highly influences the conversion gain of a mixer and its linearity). The performances of the VCO obtained with the model SLQ can be observed in Figure 4, where the phase noise, the transient simulation and the output voltage spectrum are depicted.

4. CONCLUSION

In this letter a parametric macromodel built with a sequential sampling methodology tailored for the modeling of integrated inductors was presented. This new methodology allows error measures on different performance parameters and increases the time-domain modeling accuracy. An extensive validation study has been performed, proving the improved model accuracy in L and Q estimation (with respect to models based only on S-parameter error measures). The new modeling technique has proven its value by achieving enhanced performances when used in a synthesis methodology and applied to the design of a RF circuit. Furthermore, if automated circuit design methodologies are considered, the model SLQ provides a useful technique for obtaining inductor performances estimation because of its accuracy and efficiency compared to traditional EM simulation.

ACKNOWLEDGMENTS

This work was supported in part by the TEC2013-45638-C3-3-R Project (funded by the Spanish Ministry of Economy and Competitiveness and ERDF), and in part by the P12-TIC-1481 Project (funded by Junta de Andalucia).

REFERENCES

1. C. Yue and S. Wong, Physical modeling of spiral inductors on silicon, IEEE Trans Electron Devices 47 (2000), 560–568.
2. Y. Cao, R.A. Groves, X. Huang, N.D. Zamdmer, J.-O. Plouchart, R.A. Wachnik, T.-J. King, C. Hu, Frequency-independent equivalent-circuit model for on-chip spiral inductors, IEEE J Solid State Circuits 38 (2003), 419–426.
3. G. Yang, Z. Wang, and K. Wang, Modified T-Model with an improved parameter extraction method for silicon-based spiral inductors, IEEE Trans Microwave Wireless Compon Lett 24 (2014), 817–819.
4. P. Kurgan, S. Koziel and J.W. Bandler, Low-cost EM-driven surrogate modeling and optimization of planar inductors, *IEEE MTT-S International Microwave Symposium*, 2015, pp. 1–3
5. F. Ferranti, L. Knockaert, T. Dhaene, and G. Antonini, Parametric macromodeling based on amplitude and frequency scaled systems with guaranteed passivity, Int J Numer Model Electron Networks Devices Fields 25 (2012), 139–151.
6. K. Chemmangat, F. Ferranti, T. Dhaene, and L. Knockaert, Scalable models of microwave system responses using sequential sampling on unstructured grids, Int J Numer Model Electron Networks Devices Fields 27 (2014), 122–137.
7. R. Gonzalez-Echevarria, R. Castro-López, E. Roca, F.V. Fernández, J. Sieiro, N. Vidal, J.M. López-Villegas. Automated generation of the optimal performance trade-offs of integrated inductors, IEEE Trans Comput Aided Design Integr Circuits Systems 33 (2014), 1269–1273.,
8. ADS Momentum. http://www.keysight.com/en/pc-1887116/momentum-3d-planar-em-simulator?cc=ES&lc=eng
9. B. Gustavsen and A. Semlyen, Rational approximation of frequency domain responses by vector fitting, IEEE Trans Power Delivery 14 (1999), 1052–1061.
10. J. Kennedy and R. Eberhart, "Particle swarm optimization," in *Proceedings of IEEE International Conference on Neural Networks*, vol. 4, 1995, pp. 1942–1948.
11. Cadence SpectreRF simulator. https://www.cadence.com/content/cadence-www/global/en_US/home/tools/custom-ic-analog-rf-design/circuit-simulation/spectre-rf-option.html

SUPERSTRATE LOADED MINIATURIZED PATCH FOR BIOMEDICAL TELEMETRY

Abdelrahman E. Mohamed, Ali H. Muqaibel, and Mohammad S. Sharawi

Electrical Engineering Department, King Fahd University of Petroleum & Minerals, Dhahran, 31261, Saudia Arabia; Corresponding author: msharawi@kfupm.edu.sa

Received 25 October 2016

ABSTRACT: *A Superstrate loaded miniaturized patch antenna is proposed for biomedical applications. The targeted operating frequency is (902–928 MHz) ISM band with a center frequency of 915 MHz. The antenna is designed to operate in close proximity with human-body with a size of 25 × 25 × 1.92 mm^3. Parametric studies were conducted to specify the dominant parameters and to understand their effect on the antenna performance. Measurements show that the fabricated antenna resonates around 915 MHz with a 30 MHz impedance bandwidth. On-skin measurement results are presented for several spots on the human-body. Furthermore, the transmission coefficient (S_{21}) of the fabricated antenna is measured using lean beef slices with various thicknesses and showed good agreement with simulation results.* © 2017 Wiley Periodicals, Inc.

Microwave Opt Technol Lett 59:1212–1218, 2017; View this article online at wileyonlinelibrary.com. DOI 10.1002/mop.30497

Key words: *miniaturization; biomedical antennas; small antennas; slots; superstrate*

1. INTRODUCTION

The research in the field of biomedical antennas is inspired by the need of thousands of patients relying on on-body or implanted devices to improve their lives. Antennas are utilized in biomedical applications for several purposes such as monitoring, diagnosis, power harvesting, and treatment [1]. Among Industrial, scientific, and medical band (ISM), frequency bands with the center frequencies of (433.9, 915 MHz, and 2.45 GHz) are suggested for biomedical applications. The design of a biomedical antenna shall meet the requirement of biocompatibility, miniaturization, safety, and sufficient communication properties. Patch-based antennas are preferred for on-body biomedical designs because of their low cost and profile, flexibility in design, and ease of fabrication [2].

This work focuses on biomedical antennas operating in the 915 MHz ISM band. The effect of human tissues on the radiation patterns of wearable antennas was investigated in Ref. [3]. The study focused on different polarizations of the plane wave at three frequency bands; 915 MHz, 2.45, and 5.2 GHz. In Ref. [4], an encapsulated loop antenna was proposed for health monitoring at home. The antenna was integrated with a battery and it had a diameter of 23 mm. A large truncated patch antenna was presented in Ref. [5] for off-body communications. The antenna was circularly polarized and had a size of 40 x 40 cm^2. A novel electromagnetic bandgap backed (EBG) based antenna was reported in Ref. [6]. The EBG was built by adopting split-ring resonators on a substrate size of 120 × 90 × 3 mm^3. A stretchable wire wearable antenna was proposed in Ref. [7] for biomedical applications. The proposed antenna was realized utilizing conductive filer (E-fiber) with a total size of 95.6 × 12.6 mm^2.